https://doi.org/10.1016/j.nanoen.2018.05.026
This is the Pre-Published Version.

Probing oxide-ion conduction in low-temperature SOFCs

Mingzi Sun[1], Qian He[2], Xiaojun Kuang[3], Qinyuan Zhang[2], Shi Ye[2]*, Bolong Huang[1]*

1. Department of Applied Biology and Chemical Technology, The Hong Kong Polytechnic University, Hung Hom, Kowloon, Hong Kong SAR, China

2. State Key Laboratory of Luminescent Materials and Devices, Guangdong Provincial Key Laboratory of Fiber Laser Materials and Applied Techniques, Guangzhou, 510640, China

3. Guangxi Ministry-Province Jointly-Constructed Cultivation Base for State Key Laboratory of Processing for Nonferrous Metal and Featured Materials, College of Materials Science and Engineering, Guilin University of Technology, Guilin 541004, China

*Email: msyes@scut.edu.cn (SY); bhuang@polyu.edu.hk (BH)

Nowadays, by no means fortuitous, pollution-free and bio-regenerative solid oxide fuel cells (SOFCs) have arisen to be a competitive candidate as next generation renewable energy, which exhibiting high energy efficiency and flexible fuel choices. However, fast oxide-ion transportation of electrolyte could only be ensured in high working temperature by conventional views, which can decrease the voltage loss and further determine the electrical performance of SOFCs. Herein we report an in-situ and non-contact method to monitor the working condition of SOFCs and it is potential to become a promising optical temperature sensor to detect the working temperature of electrolyte materials. With the combinative protocol between density functional theory calculation and upconversion (UC) luminescence, the entanglement between thermal-driven formed O-ion Frenkel pair (native solubilizer) and Bi^{3+} dopant (competitive inhibitor) in $La_2Mo_2O_9$ derivatives has been unraveled, especially at a lower temperature required by a future SOFCs device. It is a potential route for screening and characterizing the candidate electrolyte onsets in lower temperature without sacrificing electrical performance.

© 2018. This manuscript version is made available under the CC-BY-NC-ND 4.0 license https://creativecommons.org/licenses/by-nc-nd/4.0/

Introduction

Demands on renewable energy alternations are increasingly fierce. Solid oxide fuel cells (SOFCs) has become a competitive candidate that no charging needs to initiate operation, which also exhibits environmental benignity and high energy density. The in-system bio-circulating regenerative SOFCs have aroused huge interests, as it indeed serves as the embedded inclusion type renewable electrical generations. It has been recently applied in the deep-space exploration aircraft of China called "Lunar-Palace-One-Project". This inclusion results from their ability to optimally support the biologic internal recycle system and supply enough energy for living needs of astronauts at environment of moon, which can be attributed to recent outstanding progress on oxygen storage materials for electrodes, catalysts with high efficiency for oxygen/hydrogen generation and fast ion conductors [1-4]. Conventional views demonstrate that the high performance of SOFCs should be determined by fast ion transportation throughout the electronically insulated electrolyte [3], which can usually be achieved under high temperature environment. Hence, this caused that most ordinary electrolyte such as yttrium-stabilized zirconia (YSZ) [5-6] have to operate at least above 800 ˚C to ensure ion conduction ability. To solve the problem of such high working temperature, screening and characterizing the candidate electrolyte onsets in lower temperature without sacrificing high oxygen ion transportation ability, become urgent. Previous reports proved that native defects could be a predominant factor that controlled the oxygen ion motion of electrolyte [7], in which anion Frenkel (a-Fr) pairs are the most important one, as well as in β-$La_2Mo_2O_9$ at evaluated temperature [8-10]. Since a-Fr pairs could be dominant to influence the ion conductivity, understanding the initial formation mechanism of a-Fr pairs become significant to present research. As an intrinsic point defect in crystal structures, the formation of a-Fr pairs can be ascribed to lattice vibration under the thermal agitation as shown in Fig 1c. The discussion of a-Fr pairs in past research mainly focus on the comparison of formation energy with other point defects, where the possible initial temperature of a-Fr pairs formation has rarely been proposed before.

$La_2Mo_2O_9$ has firstly been introduced as a new fast ion conductor in 2001, which consists a poorly conductive α-phase at room temperature and highly conductive β-phase after 580 ˚C [2]. The conductivity comparison among several best-performing electrolytes with parent $La_2Mo_2O_9$ and Bi-doped β-$La_2Mo_2O_9$ are shown in Fig. 1b [2, 11-15], suggesting a very competitive conductivity at high temperature for future application. In addition, $La_2Mo_2O_9$ satisfy high ion conduction with low electron conduction for electrolyte of SOFCs due to its pure oxygen ion conductor behaviours [16]. However, the biggest challenge for its application is the stabilization of highly conductive β-phase at

lower temperature from phase change and its reactivity to NiO electrode. By using some other appropriate electrode choices such as CuO or Ni-CGO [17] can solve the problem of reaction with NiO. To stabilize and flexibly modulate the working temperature of the highly conductive β-$La_2Mo_2O_9$, dopants have been introduced to the system, which would inevitably affect the intrinsic resident and newly-formed a-Fr pairs [18-20]. Different models have been applied to $La_2Mo_2O_9$ series materials to explain their conductivity with crystallographic data from Arrhenius to the Dienes−Macedo−Litovitz (DML) model [8, 21]. By utilizing the temperature programmed isotope(TPIE) technique, Pavlova *et al.* proposed that ion motion started at around 200 ˚C, which is most possible to be the dynamically thermal-driven formed a-Fr pairs [22]. Inspired by these results, we speculate that ion conductivity of β-$La_2Mo_2O_9$ will start increasing induced by the initial formation of a-Fr pairs with a increasing concentration. Therefore, the linear relationship of ion conductivity in reference of temperature in Fig. 1b might show a turning point at around 200 ˚C based on our assumption. Therefore, a strategy to lower the working temperature of SOFCs downward range below 300 ˚C can be found if the formation mechanism of a-Fr pairs and their interaction with dopants could be revealed, and the further manipulation on working temperature can be accomplished.

Comparing with numerous experiments on studying $La_2Mo_2O_9$ with different dopants, utilizing the DFT method in exploring $La_2Mo_2O_9$ is still insufficient. Prior to probe the underlying interaction between a-Fr pairs and dopant, density functional theory (DFT) calculations have been applied to unravel the oxygen diffusion paths in $La_2Mo_2O_9$ lattice [23-24]. Partially occupied oxygen atoms with high mobility and intrinsic “free volume” of the lattice are the main contributions to the ion conductivity. Most recently, combining with quasielastic neutron scattering (QENS) method, they reveal the oxygen dynamics in the lattice based on the coordination environment change of Mo atoms [25]. In addition, the thermodynamic calculation by DFT can suggest the different temperature stage of preparation, trapping and conduction of a-Fr pairs in ion conductive materials as our previous study on $La_2Hf_2O_7$ [26], which is also essential for understanding their formation process and ion conduction in various materials.

Besides the DFT calculation method, utilizing the UC luminescence intensity ratio of $^2H_{11/2}$, $^4S_{3/2}$, $^4F_{9/2}\rightarrow{}^4I_{15/2}$ transitions of Er^{3+} might be a novel in-situ non-contact way to detect oxide-ion motion (thermal-driven formation of a-Fr pairs) in $La_2Mo_2O_9$ rather than all the other available approaches including internal friction spectroscopy [27], neutron powder diffraction [28-29] and simulation [30].

Ascribing to the thermally coupled energy levels of $^2H_{11/2}$ and $^4S_{3/2}$ with a gap of ~800 cm^{-1}, the intensity ratio of $^2H_{11/2} \rightarrow {}^4I_{15/2}$ to $^4S_{3/2} \rightarrow {}^4I_{15/2}$ transitions is independent of luminescence loss and fluctuations in excitation intensity. Thus, it linearly varies with temperature and the intensity ratio of $^4S_{3/2} \rightarrow {}^4I_{15/2}$ to these two transitions versus temperature might tell the oxide-ion jumps, which might be used as a promising optical temperature sensor to detect the formation temperature of a-Fr pairs via in-situ non-contact approach. Since a-Fr pairs might play a leading role in influencing the ion conductivity and further determining the working temperature of the electrolyte in SOFCs, this novel detecting method is a promising new approach to assist DFT in screening novel electrolyte materials with low working temperature. Driven by the necessity and potential this method, herein we report an in-situ and non-contact method to monitor the working condition of SOFCs (Fig.1) with the combination of DFT calculation for a distinct and complementary perspective on the interaction between thermal-driven formed oxide-ion Frenkel pair (native solubilizer) and Bi^{3+} dopant (competitive inhibitor) in $La_2Mo_2O_9$ derivatives, especially at a lower temperature required by a SOFCs device. As we know, innovating higher electrical performance at lower temperature mainly depends on the screening of the electrolytes.

Calculation Method

To guarantee the convergence and avoid the charge-spin out-sync sloshing, we uniformly chose the ensemble DFT (EDFT) method of Marzari *et al.* [31]. For the formation energy calculations of a-Fr pair and Bi-doped $La_2Mo_2O_9$, ultrafine quality and ultrasoft pseudopotentials with a plane-wave cutoff energy of 380 eV are chosen. Reciprocal space integration was performed using Monkhost-Pack k-point grids of 2×2×2 k-points in Brillouin zone. The geometry optimization calculations will use tolerance settings as following: total energy lower than 5.0×10^{-4} eV/atom and maximum ionic Hellmann−Feynman force lower than 0.1 eV/Å. The Broyden-Fletcher-Goldfarb-Shannon (BFGS) algorithm method has been used through all doping and defect calculations.

The a-Fr pair represents a pair of oxygen vacancy (V_O) and interstitial oxygen (I_O), which originates from separation of oxygen atom from original position to an interstitial site. Since the oxygen sites of $La_2Mo_2O_9$ are naturally occupied partially with high mobility, we will choose one oxygen atom to manually form an a-Fr pair to investigate its formation process [23, 32-33]. The chosen atom is shown in Fig. S1a, which will be put to a new interstitial position. Based on different separation distance of oxygen atom from original position, simulation models of a-Fr pair 1-7 have been built.

For doping process (Fig. S1b), there are four positions for La atoms in the lattice. We will use one Bi atom to replace the metal atom and then operate the geometry optimization for formation energy within the consistent calculation setting of a-Fr pair calculations.

Results and Discussion

Thermodynamic Calculations

The phase diagram (Fig. 2b) confirms the $La_2Mo_2O_9$ is more stable than La_2O_3 in Mo-rich environment with detailed calculation in supporting information. While high chemical potential of O indicates the substantial release of O from original equilibrium lattice sites. Thus a-Fr (O) is energetically favourable in $La_2Mo_2O_9$. Formation cost of a-Fr (Table 1) demonstrates that it can be easily formed (~0.18 eV) and even covers a wider range (0.18 eV ~ 1.90 eV).

Thermodynamic calculations are carried out by the Gibbs free energy calculations that based on the following equation:

$$\Delta G = \Delta E + \Delta ZPE - T\Delta S \quad (1)$$

where T represents the temperature and the ΔS is the change in entropy for the defect formation process. ΔE is the total energy change for the defect formation, directly obtained from our DFT calculations; ΔZPE is the change in zero-point energies of the system compared to the ideal structure. The formation of a-Fr pairs will be spontaneously start when ΔG is less than zero at specific temperature, which can be deduced from our calculation results from DFT. For example, based on the lowest formation energy (~0.18 eV) , the corresponding formation temperature should be ~468 K (Fig. 2c), showing a coincidence with the latest measurement of 200 °C by TPIE technique of Pavlova *et al.* [22]. The Gibbs free energy depends on temperature can be separated into three stages including preparation, trapping and conduction in our previous work[26]. At the preparation stage, the lattice vibration becomes more active as temperature increases, which will induce some distortion and increase the probability of forming the defects. The start of the trapping stages means that the formation of a-Fr pairs will occur spontaneously in the system. As the temperature keep increasing, more a-Fr pairs forming in the lattice, ion conduction will begin as the start of working stage. We propose that the a-Fr pair model with highest formation energy represents the most common a-Fr formation in the material, which has a corresponded working stage temperature ~700 K that also supports that the parent $La_2Mo_2O_9$ has an obvious ion conduction increase near 450 ˚C **[8]** are caused by the formation of certain amount of a-Fr pairs.

According to the definition of configuration enthalpy by Li *et al.*[34], we can also correlate the working temperature from Gibbs Free energy equation Eq. (1) with *configuration entropy S* through $S = k_B \ln W$, in which W is related with number of defect cluster in the lattice and k_B is the Boltzmann constant.

$$\Delta G = \Delta H - T\Delta S \rightarrow T = \frac{\Delta H}{\Delta S} \quad (2)$$

$$S = k_B \ln W \rightarrow dS = k_B d(\ln W) \rightarrow dS \approx k_B\left(\frac{1}{W}\right) \quad (3)$$

$$T = \frac{dH}{dS} = \left(\frac{dH}{dS}\right) W \quad (4)$$

$$T \propto E_a\left(\frac{W}{k_B}\right) \quad (5)$$

Eq. (2) is the general Gibbs Free energy equation, where H is the enthalpy and T is the temperature. According to Li's discussion on configuration entropy as Eq.(3) [34], k_B represents the Boltzmann constant and W is the number of defect cluster in the lattice that is related to the possible sites for atom. In structure as $La_2Mo_2O_9$, low symmetry results in significant number of possible sites for interstitial oxygen atoms from a-Fr pairs. Thus, the difference between the change of W for oxygen atoms in same lattice should be neglect and further simplify Eq. (3) as shown. Apply Eq. (3) into Eq. (2) can generate Eq. (4). In addition, we propose that enthalpy change for a-Fr equals to the activation energy, so we can derive Eq. (5). Then the working temperature is in direct proportion to the activation energy, which is also shown in Fig.2b. Therefore, the higher disordered structure will lead to lower activation energy and further lower the working temperature of materials.

Electronic Properties

The projected density of states (PDOS) of a-Fr pairs and Bi^{3+} in $La_2Mo_2O_9$ models are displayed in similar pattern that reveal that they won't impose obvious influence on electronic properties (Fig. 2d-2e). Formation of a-Fr pair will pin the Fermi level at mid-gap, and Bi^{3+} will drag Fermi level slightly closer to valence band maximum (VBM), both meaning that $La_2Mo_2O_9$ will still maintain electronically insulated that is suitable for electrolyte material. Fig. 1d shows the orbital diagram for the gap states appear in Fig. 2d, where the contribution only from the Mo atoms instead of O atoms

from a-Fr pairs. This also support that the formation of a-Fr pairs will not change the electronic properties of $La_2Mo_2O_9$. More detailed discussion can be seen in supporting information.

Formation Energy of a-Fr and dopants

For a-Fr pairs, the formation energy calculations will be conducted based on Eq. (1) as following and the results are shown in Table 2:

$$E_{form}^{q} = E_{Defect} - E_{bulk} + \sum(n_i E_i + n_i \mu_i) + qE_F \quad (6)$$

A-Fr pairs show a large range of formation energy from 0.18 eV to 1.90 eV, meaning that a-Fr pair is possible to form at lower temperature because of low energy barrier, which originates from the low symmetrical crystal structure of $La_2Mo_2O_9$. However, a-Fr pairs with higher formation energy might represent the most common presence of a-Fr pairs that caused the start of ion conduction. Moreover, we have investigated the relationship of formation of a-Fr pairs with local atom environment in terms of average coordination number as shown in Fig. 2a. Notably, La atoms have higher coordination numbers than Mo atoms, implying more complicated local environment. Within the formation of a-Fr pairs defects in the material, the average coordination number of La atoms will experience change from 6.50 to even 7.50, implying obvious local structural change. In contrast, Mo atoms maintain the average coordination numbers at the range from 4.50 to 4.75, suggesting local environment has not been affected significantly. Hence, more La-O bonds are believed to play a role as affecting the stability of local environment. For the formation energy of Bi doped $La_2Mo_2O_9$, formation energy will be also calculated using same equation under chemical potential environment from Fig. 2b and results of Bi doping on La sites(Bi_{La}) and Mo sites (Bi_{Mo}) are both compared in Table 2. Lacorre [35] has proposed the lone pair substitution theory for finding proper dopants and illustrated that the doping process will be greatly affected by the ionic radius difference. Apparently, Bi_{Mo} does not satisfy the LPS concept due to the huge difference in both valence state and ionic radius between Bi and Mo. As the formation energy shown, Bi_{Mo} models reflect much higher formation energy than Bi_{La}, representing that higher difficulty to realize in actual experiments. For Bi_{La}, the formation energies are similar on different La sites except one position. This can be ascribed to the highest coordination number of La at this site, which increase the difficulty of replacing the original La atom at the stable environment. The largest number of La-O bonds at this site are believed that undertake the role of stabilizing the lattice.

Interaction between Dopant Bi and a-Fr pairs

The interaction of additional dopants Bi^{3+} and intrinsic a-Fr pairs is necessary to investigate for achieving the modulation of electrical properties of $La_2Mo_2O_9$. Combining the results of formation energies and electronic properties, we have found that the formation of a-Fr pairs and Bi_{La} will greatly affect each other in the $La_2Mo_2O_9$ lattice and play roles as the "native-solubilizers" the "competitive inhibitor", respectively. As a native point defect, a-Fr pair will be easily formed with low energy barrier. Thus, the influence on external dopant Bi entering the lattice with the existence of a-Fr pair has been calculated in Table S1. It is found that the formation energies of Bi_{La} with a-Fr pair have been reduced when comparing with the average formation energy of those models without a-Fr pairs. These demonstrate that the a-Fr pairs as native solubilizers in the lattice can attenuate the barrier for Bi doping and diffusing into the internal lattice instead of accumulating near the surface of material. This can be explained that a-Fr pairs could affect the space structure that lead to a reduced energy barrier for dopant Bi to replace La atom. Inversely, Bi_{La} in lattice will impose an inhabitation effect on the newly formed a-Fr pairs, which can be clearly seen in Table 3 and Fig. 2f. The formation energies cost of a-Fr pairs at the same location will have an evident increase than $La_2Mo_2O_9$ without dopants. Within the presence of Bi_{La}, the formation energies needed to form the a-Fr pair in the lattice have significantly increased ranging from 14 % up to even 540 % that might result in the loss of advantages in formation. The largest formation energy increment is achieved at the lowest formation energy cost a-Fr pair that form around 200 ˚C. With combination of Gibbs free energy calculations, the increment of formation energy also is accompanied with visible enhancement of formation temperature of a-Fr pair, which increase from the 468K~700K to 560 K~1020 K (Fig. 2g). This elucidates that the formation requirements for a-Fr pairs have become much more difficult due to the presence of Bi_{La}. As an important component of ion conductivity, increasing the formation energy cost and temperature of a-Fr pairs will further impede the ion diffusion. Consequently, we propose that the competitive behaviors between Bi_{La} and a-Fr pairs in lattice will lead to two different mechanisms. In Fig. 2h, even when Bi concentration reaches the limits, the formation energies of Bi_{La} is still higher than a-Fr pairs and results in a dynamic balance until the synthetization ends. In the inset, the comparison of velocity of reaction with and without inhibitor has shown. In Fig. 2i, another mechanism shows that if the Gibbs energies of Bi_{La} decrease a lower level than the formation of a-Fr pairs that breaks the balance in Fig. 2h, then Bi_{La} will significantly suppress the formation of a-Fr pairs in the lattice. The concentration of Bi will keep increasing until the doping limits. The change of energy barrier of Gibbs energies has been illustrated in the inset Therefore, as the dopant Bi concentration keep increasing to a certain level,

the ion conductivity will be restricted because the formation of a-Fr pairs has been largely suppressed.

UC Luminescence Experiments

Experimentally, we attempt to reveal the effects of Bi doping on the thermal-driven oxide-ion jump (formation of new a-Fr pairs) via the UC luminescence based on the sensitive nature of luminescence of Er^{3+} to the variation of local crystal field and AC impedance spectroscopy at low temperature. The synthetization method detailed has been provided in the supporting material. Several different characterization methods have been used to verify the stabilization of β-$La_2Mo_2O_9$. Fig. 3a presents the room temperature XRD patterns of $La_{2-x}Bi_xMo_2O_9$ (x = 0, 0.05, 0.15, 0.3) samples and the standard XRD patterns of cubic β-$La_2Mo_2O_9$ (ICSD98871). The inset of Fig. 3(a) is enlarged pseudo-cubic (231) diffraction line. It is reported that the monoclinic α-$La_2Mo_2O_9$ has several splitting peaks for the pseudo-cubic reflection (231) at around 2θ = 46-49°[36-37], while the peaks in the inset seems to be different from that of monoclinic α-$La_2Mo_2O_9$. Besides XRD, Raman spectroscopy is another powerful tool to provide supporting evidence of β-$La_2Mo_2O_9$[28, 37-39]. Fig. 3b-3c shows Raman spectra for $La_{2-x}Bi_xMo_2O_9$ (x = 0, 0.05, 0.15, 0.3) at room temperature. The band at 700-1000 cm^{-1} is the determining information about the structure transformation[38]. For the β-$La_2Mo_2O_9$, there should be a significant change with only two apparent peaks, while for the α-$La_2Mo_2O_9$ phase there are at least four apparent distinguished peaks. The two peaks at around 797 cm^{-1} (Peak 1) and 922 cm^{-1} (Peak 2) are broadened or diminished with doping Bi, indicating that the doped samples are in β form[39-41]. Thus, the crystallographic information confirm that the cubic structure is stabilized for doping Bi, which is similar with the previous research[21, 28, 36-39, 42-43].

The internal friction(IF) spectra of $La_{2-x}Bi_xMo_2O_9$ (x = 0.15, 0.3) have shown in Fig. S4a-S4b under four different frequency. Both samples show a broad peak at around 175 ºC. The relaxation parameters obtained from these peaks are close to those short-range ion diffusion behaviors in electrolyte YSZ and other oxides [44]. High ionic conductivity of $La_2Mo_2O_9$ related materials can be attributed to native oxygen vacancies in the lattice, which can supply sufficient space for oxygen ion diffusion. In Fig. S5, the impedance spectra of $La_{2-x}Bi_xYb_{0.06}Er_{0.04}Mo_2O_9$ (x = 0.05, 0.15, 0.3) at different temperature are displayed. Inset of Fig. S5 is the equivalent circuit, in which R and CPE represent the resistance and constant phase element of bulk, grain boundary and electrode, respectively. The results that the conducting species in $La_{2-x}Bi_xYb_{0.06}Er_{0.04}Mo_2O_9$ should be

predominate oxygen ions [45-46]. To further compare the dependence of ion conductivity on Bi dopant concentration, the Raman spectra dependence on temperature has been conducted for sample $La_{2-x}Bi_xMo_2O_9$ with x = 0.15 and 0.30 in Fig. S6. The different change of the peak positions and half-peak width near 150 ºC implies the influence from the suppression of formation of a-Fr induced by higher dopant concentration of Bi in the lattice. More detailed results are discussed in the supporting information.

Typical UC emission spectra of $La_{1.75}Bi_{0.15}Yb_{0.06}Er_{0.04}Mo_2O_9$ recorded at different temperature are illustrated in Fig. 4a. All the samples exhibit bright and shining UC luminescence at room temperature upon excitation of 980 nm diode laser. The green emission peaks at ~525 nm and ~550 nm can be attributed to the $^2H_{11/2}\rightarrow{}^4I_{15/2}$ and $^4S_{3/2}\rightarrow{}^4I_{15/2}$, respectively, while the red emission peak at ~660 nm is ascribed to the $^4F_{9/2}\rightarrow{}^4I_{15/2}$ transitions of Er^{3+}. All the other samples ($La_{1.9-x}Bi_xYb_{0.06}Er_{0.04}Mo_2O_9$ (x = 0.05, 0.3) all show similar spectra. The absolute emission intensities of lanthanide ions are greatly influenced by many factors including the grain sizes, the light-focused domain sizes, pumping power density, fluctuation of light source and spectrometers, and so on [30, 47-48]. Therefore, it should be more convincing by using the relative integrated intensity ratios of the three emission peaks of Er^{3+} (I_{525}, I_{550}, I_{660}) to evaluate the temperature effect on UC luminescence. Owing to the small energy gap of about 800 cm^{-1} between the $^2H_{11/2}$ and $^4S_{3/2}$ levels, the $^2H_{11/2}$ level can be easily populated from $^4S_{3/2}$ level through thermal agitation, leading to variation in the $^2H_{11/2}\rightarrow{}^4I_{15/2}$ and $^4S_{3/2}\rightarrow{}^4I_{15/2}$ transitions of Er^{3+} at different temperature [30, 47-48]. Their intensity ratio versus temperature in Ln~1/T plot should be linear, which is the base of optical temperature sensing application [49-52]. This linear line could be utilized to evaluate the working temperature of $La_2Mo_2O_9$:Bi,Yb,Er electrolytes as reference with the detected UC emission intensity ratio in the proposed low-temperature SOFCs. The detailed calculation method of the two green UC emissions can be found in SI. The fitting linear relationship between UC luminescence intensity and temperature can be seen in Fig. 4b and Fig. 4c, which is the base of optical temperature sensing application [49-53]. The sensitivity of the sensor is increasing as temperature increases can be clearly reflected in Fig. 4d. Herein, this linear behavior is further applied to be an internal reference to characterize the other two lognormal plots of UC emission intensity ratios, as depicted in Fig. 5a-5c. It is very evident that there is a turning point at ~150°C in all the samples with different concentration of Bi except for $La_{1.6}Bi_{0.3}Yb_{0.06}Er_{0.04}Mo_2O_9$, which not only represents the detection of ion motion as previous work [30] but can support our previous DFT results that Bi dopant will suppress the thermal-driven formation of a-Fr pairs especially when reaching certain concentration.

Contrast experiment on dopant Mg in oxide-ion conductor $LaGaO_3$ in Fig. S7 also support same assumption. These results also suggest that the Er^{3+} could sense obvious variation of surrounding chemical environment, which probably ascribed to the thermal-driven formation of new a-Fr pairs.

AC impedance spectroscopy is also recorded as a reference of oxide-ion motion throughout electrolyte lattice because the permittivity value at 10^{-7}~10^{-5} F•cm^{-1} of electric double layers formed between electrodes can tell the long-range oxide-ion motion [54]. Fig. 5d-5f present the permittivity of ($La_{1.9-x}Bi_xYb_{0.06}Er_{0.04}Mo_2O_9$ (x = 0.05, 0.15, 0.3) ceramic pellets as a function of frequency at different temperature [54]. All samples possess a permittivity lower than ~10^{-6} F•cm^{-1} at 300°C, manifesting that the oxide-ion motion below 300°C exists but is not efficient enough to support effective ion transportation for electrolyte. $La_{1.6}Bi_{0.3}Yb_{0.06}Er_{0.04}Mo_2O_9$ even shows the lowest permittivity than ~10^{-7} F•cm^{-1} at 300°C, which is in good agreement with former UC emission results. These findings demonstrate that a-Fr pair formation starts at low temperature, but it can only generate enough ion conductivity until high temperature, which is consistent with our assumption.

The enlarged 525 nm and 550 nm emission decay curves (original data shown in Fig. S8) of $La_{1.75}Bi_{0.15}Yb_{0.06}Er_{0.04}Mo_2O_9$ in Fig. S9a and S9c also show a distinct decrease at above 150°C, which is analogous with previous report [30] and suggests that there should be oxide-ion jumps in this sample when temperature is above 150°C. Similar to the UC luminescence intensity in reference of temperature, the $La_{1.6}Bi_{0.3}Yb_{0.06}Er_{0.04}Mo_2O_9$ reflects different behavior with faster decay and no significant rise-up at the early stage of decay in Fig. S8b and S8d. Associating with the absence of break point in lognormal plots of UC emission intensity ratios and low permittivity at temperature below 300°C, we can also preliminarily speculate that the ion motion caused by a-Fr defects is inefficient in $La_{1.6}Bi_{0.3}Yb_{0.06}Er_{0.04}Mo_2O_9$, which supports our DFT assumption on the relationship between Bi dopants and a-Fr pairs. Therefore, the behavior of slopes above the temperature of the break points could be applied as potential sensor to detect the ion conduction of electrolyte in SOFCs. The temperature-dependent grain conductivities of $La_{1.9-x}Bi_xYb_{0.06}Er_{0.04}Mo_2O_9$ (x = 0.05, 0.15, 0.3) (Fig. S9c) reveals that both the conductivity and the activation energy will be reduced with enhancement of Bi contents when fitting the data in Arrhenius regime, meaning a-Fr pairs motion in electrolyte lattice will be hindered and further suppress the conductivity as the Bi dopants concentration increased. Hence, the significantly decreases of conductivity of $La_{1.6}Bi_{0.3}Yb_{0.06}Er_{0.04}Mo_2O_9$ can be attributed to the inhabitation effect of Bi^{3+} on a-Fr formation with

the lone pair of Bi^{3+} ion blocks the oxide-ion migration. The lower value of activation energy could be ascribed to the narrower gap between the VBM and CBM as revealed by DFT calculation.

Summary

In this work, we utilize DFT calculation methods assisted by UC luminescence characterization method as a novel non-contact approach to unravel the interaction between intrinsic a-Fr pairs defects and additive Bi dopants in $La_2Mo_2O_9$. The Bi dopants have been found that play an "inhibitor" role on hindering the formation of a-Fr pairs and further affect the ion conductivity if reaches certain concentration. Meanwhile the presence of a-Fr pairs will benefit the actualization of Bi doping process. This UC luminescence method also supports our calculation results, which can inspire and guide future design on detecting the working temperature of SOFCs system. Furthermore, combining DFT calculation with UC luminescence characterization method enable us to predict, characterize electronic properties of novel materials to screen out potential electrolytes that works in low temperature for high-efficiency multi-channel ion conduction system in fields of SOFCs. Therefore, we think that the present work possesses the significant research results for impacting the frontier renewable energy research in a timely manner.

Table 1

Table 1 Formation energies of a-Fr pair defects and Bi doping at different positions under Mo rich environment

Compound Model	Formation Energy (eV)
a-Fr -1	0.182
a-Fr -2	0.407
a-Fr -3	0.622
a-Fr -4	0.629
a-Fr -5	1.241
a-Fr -6	1.332
a-Fr -7	1.970

Table 2

Table 2 Formation energies of Bi doping at different positions under Mo rich environment

Compound Model	Formation Energy (eV)
$La_{1.5}Bi_{0.5}Mo_2O_9$ -1	1.040
$La_{1.5}Bi_{0.5}Mo_2O_9$ -2	0.898
$La_{1.5}Bi_{0.5}Mo_2O_9$ -3	0.913
$La_{1.5}Bi_{0.5}Mo_2O_9$ -4	4.617
$La_2Mo_{1.5}Bi_{0.5}O_9$-1	5.373
$La_2Mo_{1.5}Bi_{0.5}O_9$-2	8.489
$La_2Mo_{1.5}Bi_{0.5}O_9$-3	2.640
$La_2Mo_{1.5}Bi_{0.5}O_9$-4	7.154

Table 3

Table 3 Formation energies of Bi doping in $La_2Mo_2O_9$ with a-Fr pair models at different position (related to models in Table S1)

Model	Formation Enthalpy without Bi_{La} (eV)	Formation Enthalpy with Bi_{La} (eV)
a-Fr -1	0.182	1.171
a-Fr -2	0.407	1.364
a-Fr -3	0.622	1.647
a-Fr -4	0.801	4.727
a-Fr -5	1.241	2.384
a-Fr -6	1.331	1.504
a-Fr -7	1.970	1.299

Figure 1

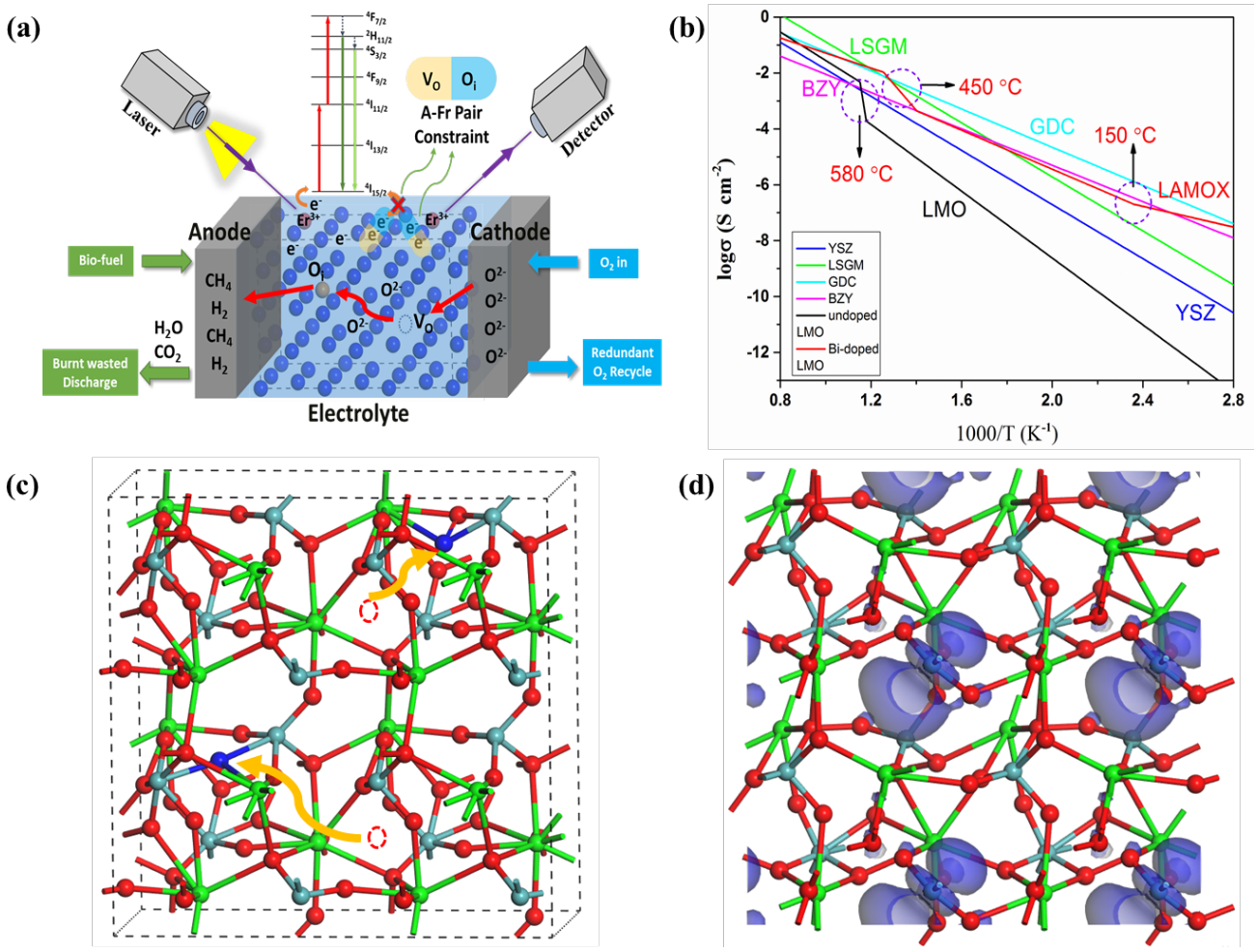

Fig. 1. (a) The schematic diagram illustrates the application of low temperature SOFCs and in-situ characterization technique *via* non-contact UC luminescence. (b) The ion conductivity comparison of the several electrolytes for SOFCs. (c) Illustration of formation of a-Fr pairs in the lattice. (d) Local view of relaxed structure of $La_2Mo_2O_9$ with a-Fr pairs. The blue surface denoted to electrons localized on the d orbitals of Mo atom and therefore inducing symmetrical gap states pair pinned at Fermi level in dos diagram.

Figure 2

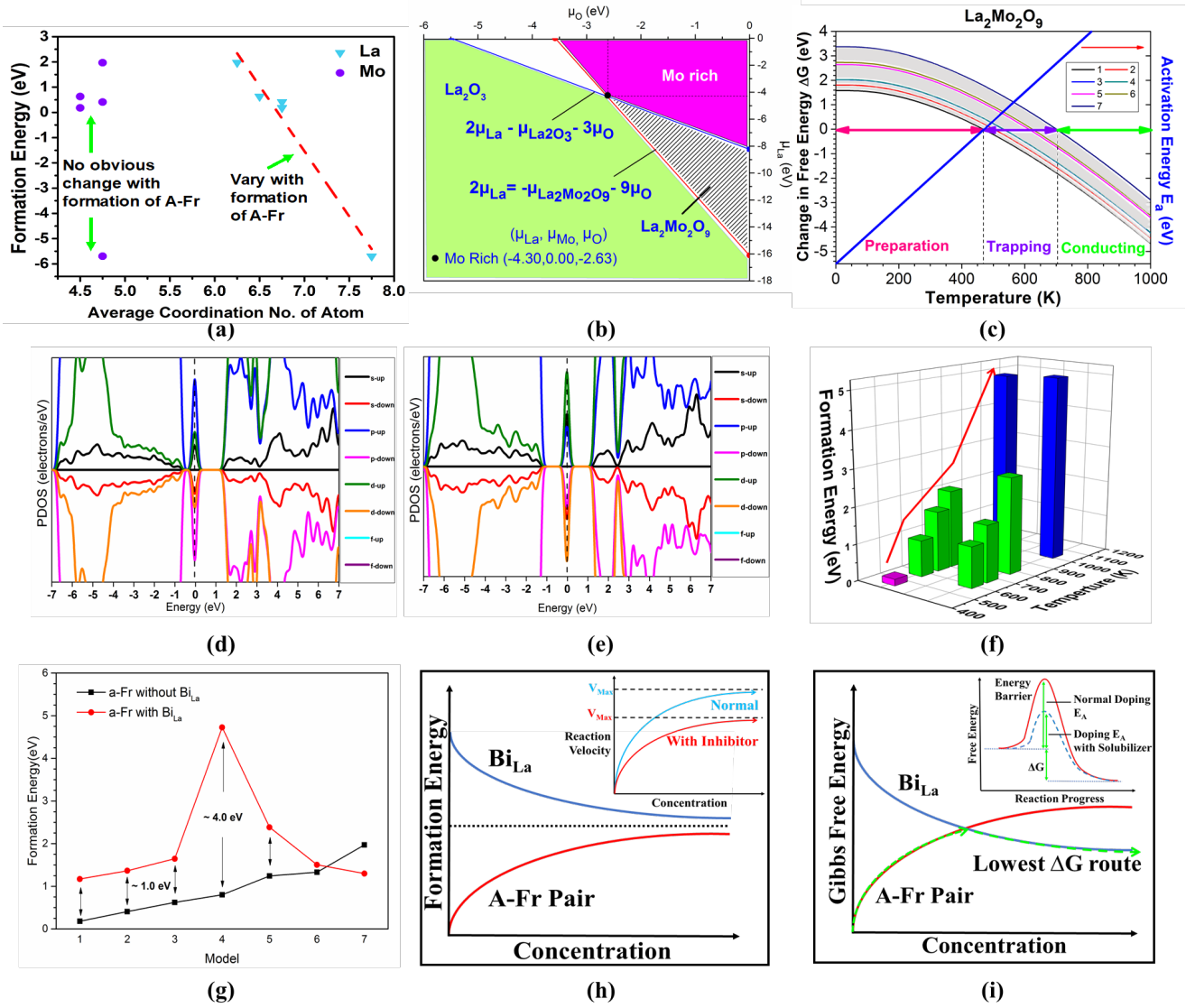

Fig. 2. (a) The fitting linear between coordination number of La and formation energy of a-Fr pair in $La_2Mo_2O_9$. (b) Diagram of possible values of La and O chemical potentials under Mo rich environment (striped shaded region) defining the stability of $La_2Mo_2O_9$. The chemical potentials μ_{La}, μ_O are limited by the formation of La_2O_3 secondary phases and $La_2Mo_2O_9$. The filled black circle corresponds to $\mu_{La} = -4.30$ eV and $\mu_O = -2.625$ eV. (c) The ΔG with consideration of the a-Fr pairs in $La_2Mo_2O_9$ system. Formation of a-Fr pairs starts from 468 K~ 700 K. Blue solid line represents that the activation energy of a-Fr pair should in direct proportion to working temperature. (d) The PDOS of $La_2Mo_2O_9$ with lowest formation energy of a-Fr pair. (e) The PDOS of $La_2Mo_2O_9$ of Bi_{La}. (e) DFT calculations on formation energy and temperature of chosen a-Fr pairs models after introducing Bi_{La}. Each pair of the column represents same a-Fr pairs model with Bi_{La} at two different La positions, which all show very similar formation environment. Pink column represents the lowest formation energy of a-Fr model with lowest formation temperature that starts at 468 K. (g) The comparison of

formation energies of a-Fr pairs with and without dopant Bi. (h)-(i) Proposed effect of dopant-Bi and a-Fr pairs.

Figure 3

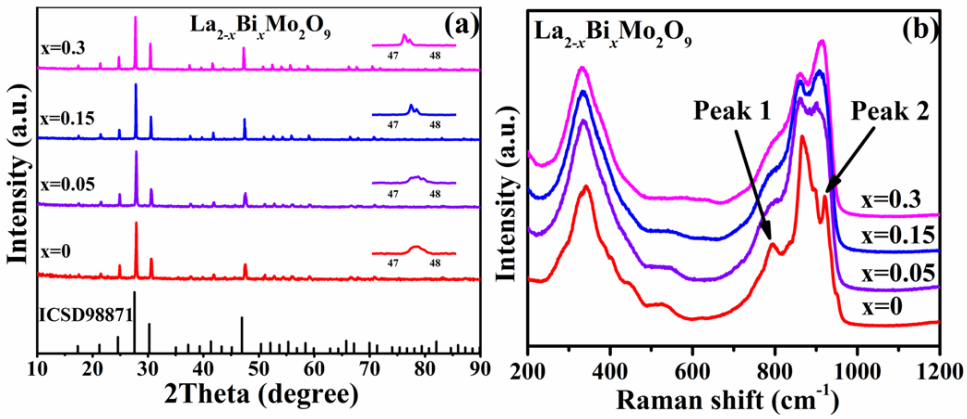

Fig. 3 (a) XRD patterns of $La_{2-x}Bi_xMo_2O_9$ (x = 0, 0.05, 0.15, 0.3) samples recorded at room temperature, along with the reference of cubic β-$La_2Mo_2O_9$ (ICSD98871), inset: the enlarged pseudo-cubic (231) peaks, Raman spectra for (b) $La_{2-x}Bi_xMo_2O_9$ (x = 0, 0.05, 0.15, 0.3) at room temperature.

Figure 4

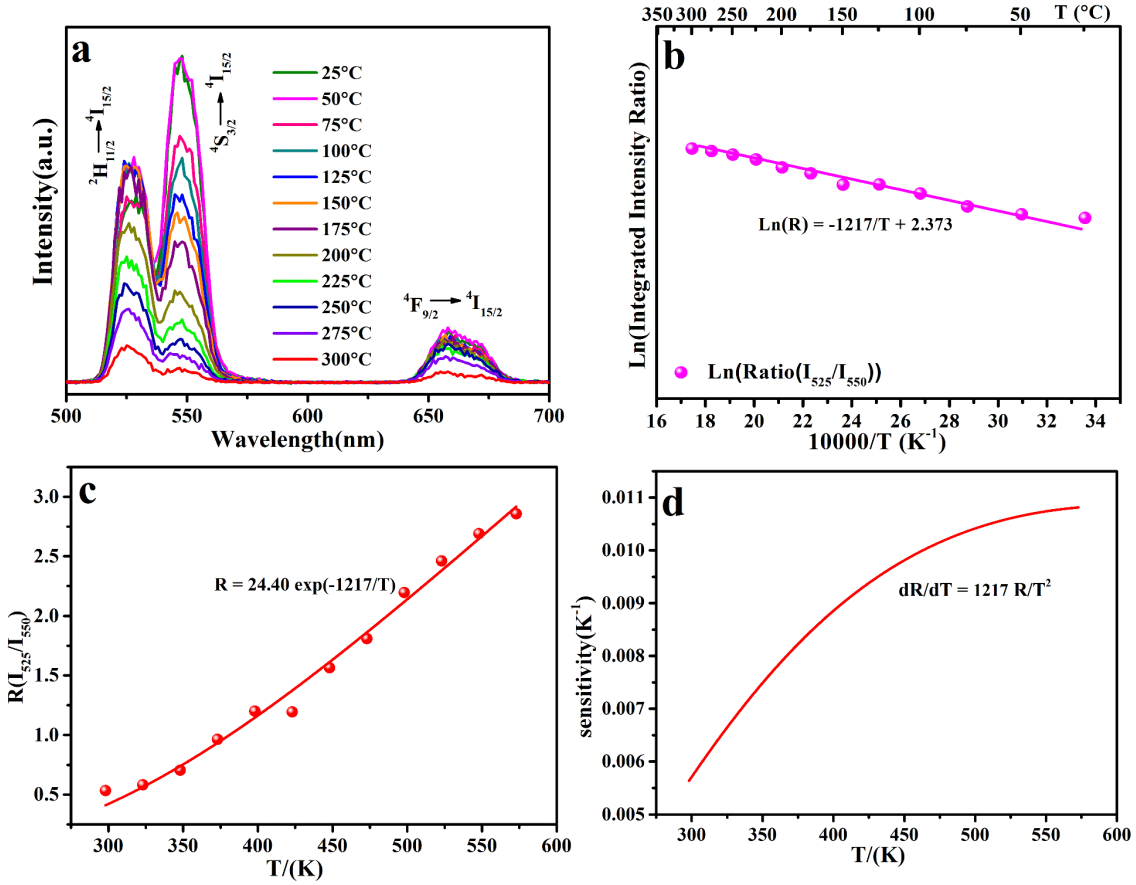

Fig. 4. (a) Temperature-dependent UC emission spectra of $La_{1.75}Bi_{0.15}Yb_{0.06}Er_{0.04}MoO_9$ under excitation of a 980nm laser beam (about ~180 mW mm^{-2}); (b) Monolog plot of the intensity ratio of the 525 and 550 nm emission peaks as a function of inverse absolute temperature. (c) Intensity ratio of the 525 and 550 nm emission peaks versus the temperature. (d) Sensitivity as a function of the temperature.

Figure 5

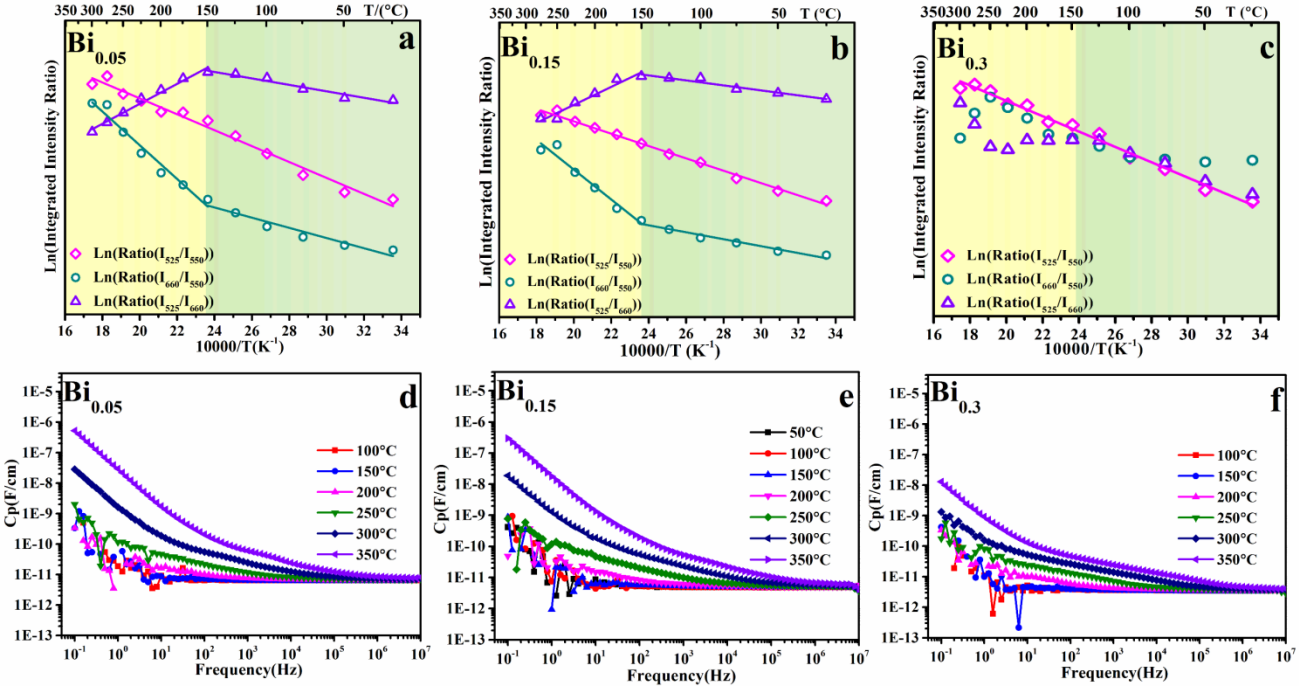

Fig. 5. (a)-(c) Lognormal plot of the intensity ratio of I_{525}/I_{550}(Ln(Ratio(I_{525}/I_{550}))), I_{660}/I_{550}(Ln(Ratio(I_{660}/I_{550}))) and I_{525}/I_{660}(Ln(Ratio(I_{525}/I_{660}))) as a function of inverse absolute temperature of $La_{1.9-x}Bi_xYb_{0.06}Er_{0.04}Mo_2O_9$ (x = 0.05, 0.15, 0.3), these are the fitted lines. (d)-(f) Permittivity of $La_{1.9-x}Bi_xYb_{0.06}Er_{0.04}Mo_2O_9$ (x =0.05, 0.15, 0.3) ceramic pellets as a function of frequency at different temperatures.

References

[1] Y. H. Huang; R. I. Dass; Z. L. Xing; J. B. Goodenough, Double Perovskites as Anode Materials for Solid-Oxide Fuel Cells. *Science* **2006,** *312* (5771), 254-7.

[2] P. Lacorre; F. Goutenoire; O. Bohnke; R. Retoux; Y. Laligant, Designing Fast Oxide-Ion Conductors Based on $La_2mo_2o_9$. *Nature* **2000,** *404* (6780), 856-858.

[3] A. J. Jacobson, Materials for Solid Oxide Fuel Cells. *Chem Mater* **2010,** *22* (3), 660-674.

[4] J. M. Serra; H.-P. Buchkremer, On the Nanostructuring and Catalytic Promotion of Intermediate Temperature Solid Oxide Fuel Cell (It-Sofc) Cathodes. *J Power Sources* **2007,** *172* (2), 768-774.

[5] S. P. S. Badwal, Yttria Tetragonal Zirconia Polycrystalline Electrolytes for Solid State Electrochemical Cells. *Applied Physics A Solids and Surfaces* **1990,** *50* (5), 449-462.

[6] S. Badwal, Zirconia-Based Solid Electrolytes: Microstructure, Stability and Ionic Conductivity. *Solid State Ionics* **1992,** *52* (1-3), 23-32.

[7] X. Kuang; M. A. Green; H. Niu; P. Zajdel; C. Dickinson; J. B. Claridge; L. Jantsky; M. J. Rosseinsky, Interstitial Oxide Ion Conductivity in the Layered Tetrahedral Network Melilite Structure. *Nat Mater* **2008,** *7* (6), 498-504.

[8] G. Corbel; A. Selmi; E. Suard; P. Lacorre, “Free” Volume Expansion and Formation Enthalpy of Defects as Key Parameters Tuning the Oxide Ionic Conductivity in Derivatives of B-$La_2mo_2o_9$. *Chem Mater* **2014,** *26* (23), 6838-6851.

[9] M. Sun; B. Huang, "Energy Selection Channels" for High-Performance Electrolyte: Anion-Frenkel Defect Pair as Dominant Source for O Ion Conductions in Pyrochlore-Type Lanthanide Hafnium Oxides Sofc. *Inorg Chem* **2017,** *56* (14), 7975-7984.

[10] P. Wilde; C. Catlow, Defects and Diffusion in Pyrochlore Structured Oxides. *Solid State Ionics* **1998,** *112* (3-4), 173-183.

[11] B. C. Steele; A. Heinzel, Materials for Fuel-Cell Technologies. *Nature* **2001,** *414* (6861), 345-52.

[12] T. Ishihara; T. Shibayama; M. Honda; H. Nishiguchi; Y. Takita, Intermediate Temperature Solid Oxide Fuel Cells Using $Lagao_3$ Electrolyte Ii. Improvement of Oxide Ion Conductivity and Power Density by Doping Fe for Ga Site of $Lagao_3$. *J Electrochem Soc* **2000,** *147* (4), 1332-1337.

[13] V. Esposito; E. Traversa, Design of Electroceramics for Solid Oxides Fuel Cell Applications: Playing with Ceria. *J Am Ceram Soc* **2008,** *91* (4), 1037-1051.

[14] D. Pergolesi; E. Fabbri; A. D'Epifanio; E. Di Bartolomeo; A. Tebano; S. Sanna; S. Licoccia; G. Balestrino; E. Traversa, High Proton Conduction in Grain-Boundary-Free Yttrium-Doped Barium Zirconate Films Grown by Pulsed Laser Deposition. *Nat Mater* **2010,** *9* (10), 846-52.

[15] V. Voronkova; E. Kharitonova; A. Krasilnikova, Phase Transitions and Electrical Conductivity of Bi-Doped $La_2mo_2o_9$ Oxide Ion Conductors. *physica status solidi (a)* **2009,** *206* (11), 2564-2568.

[16] W. Liu; W. Pan; J. Luo; A. Godfrey; G. Ou; H. Wu; W. Zhang, Suppressed Phase Transition and Giant Ionic Conductivity in $La_2mo_2o_9$ Nanowires. *Nat Commun* **2015,** *6*, 8354.

[17] G. Corbel; P. Lacorre, Compatibility Evaluation between La2mo2o9 Fast Oxide-Ion Conductor and Ni-Based Materials. *J Solid State Chem* **2006,** *179* (5), 1339-1344.

[18] M. A. Howard; O. Clemens; K. S. Knight; P. A. Anderson; S. Hafiz; P. M. Panchmatia; P. R. Slater, Synthesis, Conductivity and Structural Aspects of $Nd_3zr_2li_{7-3x}al_xo_{12}$. *Journal of Materials Chemistry A* **2013,** *1* (44), 14013-14022.

[19] G. C. Mather; M. S. Islam, Defect and Dopant Properties of the $Srceo_3$-Based Proton Conductor. *Chem Mater* **2005,** *17* (7), 1736-1744.

[20] J. J. Carey; M. Nolan, Influence of Trivalent Doping on Point and Frenkel Defect Formation in Bulk Chromium (Iii) Oxide. *Solid State Ionics* **2017,** *307*, 51-64.

[21] G. l. Corbel; E. Suard; P. Lacorre, Structural Key of the Thermal Expansion and the Oxide Ionic Conduction in Derivatives of $La_2mo_2o_9$: A Temperature-Controlled Neutron Diffraction Study of B-$La_{1.7}bi_{0.3}mo_2o_9$. *Chem Mater* **2011,** *23* (5), 1288-1298.

[22] S. Pavlova; Y. Bespalko; V. Sadykov; N. Eremeev; T. Krieger; E. Sadovskaya; A. Ishchenko; A. Bobin; A. Ulihin; N. Uvarov; A. Smirnova, Structural and Transport Properties of Doped Lamox — Electrolytes for It Sofc. *Solid State Ionics* **2016,** *288*, 103-109.

[23] C. J. Hou; Y. D. Li; P. J. Wang; C. S. Liu; X. P. Wang; Q. F. Fang; D. Y. Sun, Oxygen-Ion Arrangements and Concerted Motion in B−$La_2mo_2o_9$. *Physical Review B* **2007,** *76* (1), 014104-014109.

[24] H. Chun-Ju; Z. Xu; L. Chang-Song; W. Xian-Ping; F. Qian-Feng, Crystal Structure of B-$La_2mo_2o_9$ from First Principles Calculation. *Chinese Physics Letters* **2008,** *25* (9), 3342-3345.

[25] J. R. Peet; C. A. Fuller; B. Frick; M. Zbiri; A. Piovano; M. R. Johnson; I. R. Evans, Direct Observation of Oxide Ion Dynamics in La2mo2o9on the Nanosecond Timescale. *Chemistry of Materials* **2017,** *29* (7), 3020-3028.

[26] M. Sun; B. Huang, Comparison and Correlation of Structural Disorder Caused by Anion Frenkel in Affecting Ion Conduction of $La_2hf_2o_7$ and $La_2mo_2o_9$ as High Performance Electrolytes in Sofcs. *MRS Advances* **2017,** *2* (54), 3317-3322.

[27] C. Tealdi; G. Chiodelli; L. Malavasi; G. Flor, Effect of Alkaline-Doping on the Properties of $La_2mo_2o_9$ Fast Oxygen Ion Conductor. *J Mater Chem* **2004,** *14* (24), 3553-3557.

[28] T. Paul; A. Ghosh, Structure and Vibrational Properties of $La_{2-X}bi_xmo_2o_9$ ($0.05\leqslant X\leqslant 0.4$) Oxygen Ion Conductors. *J Alloys Compd* **2014,** *613*, 146-152.

[29] L. H. Fischer; G. S. Harms; O. S. Wolfbeis, Upconverting Nanoparticles for Nanoscale Thermometry. *Angewandte Chemie-International Edition* **2011,** *50* (20), 4546-4551.

[30] Y. Li; X. F. Jiang; F. Q. Tao; Y. M. Yang; Q. Y. Zhang; S. Ye, Detection of Oxide-Ion and Oxygen Vacancy Swapping Via Upconversion Luminescence in $La_2mo_2o_9$:Yb^{3+}, Er^{3+}. *Journal of Materials Chemistry C* **2016,** *4* (30), 7286-7293.

[31] N. Marzari; D. Vanderbilt; M. C. Payne, Ensemble Density-Functional Theory for *Ab Initio* Molecular Dynamics of Metals and Finite-Temperature Insulators. *Phys Rev Lett* **1997,** *79* (7), 1337-1340.

[32] J. Shamblin; M. Feygenson; J. Neuefeind; C. L. Tracy; F. Zhang; S. Finkeldei; D. Bosbach; H. Zhou; R. C. Ewing; M. Lang, Probing Disorder in Isometric Pyrochlore and Related Complex Oxides. *Nat Mater* **2016,** *15* (5), 507-11.

[33] T. Paul; A. Ghosh, Conduction and Relaxation Mechanisms in Bismuth Doped $La_2mo_2o_9$ Ionic Conductors. *J Appl Phys* **2013,** *114* (16), 164101-164108.

[34] Y. Li; W. G. Schmidt; S. Sanna, Intrinsic Linbo3 Point Defects from Hybrid Density Functional Calculations. *Physical Review B* **2014,** *89* (9), 094111-094118.

[35] P. Lacorre, The Lps Concept, a New Way to Look at Anionic Conductors. *Solid State Sciences* **2000,** *2* (8), 755-758.

[36] L. Haoran; W. Chang-An; M. A. White, Complex Effect of Sm^{3+}/W^{6+}Codoping on A-B Phase Transformation and Phonon Scattering of Oxygen-Deficient $La_2mo_2o_9$. *J Am Ceram Soc* **2015,** *98* (5), 1385-1388.

[37] M. Guzik; M. Bieza; E. Tomaszewicz; Y. Guyot; G. Boulon, Development of Nd^{3+}-Doped Monoclinic Dimolybdates $La_2mo_2o_9$ as Optical Materials. *Zeitschrift für Naturforschung B* **2014,** *69* (2), 193-204.

[38] M. Guzik; M. Bieza; E. Tomaszewicz; Y. Guyot; E. Zych; G. Boulon, Nd^{3+} Dopant Influence on the Structural and Spectroscopic Properties of Microcrystalline $La_2mo_2o_9$ Molybdate. *Opt Mater* **2015,** *41*, 21-31.

[39] W. Liu; W. Pan; J. Luo; A. Godfrey; G. Ou; H. Wu; W. Zhang, Suppressed Phase Transition and Giant Ionic Conductivity in La2mo2o9 Nanowires. *Nature Communications* **2015,** *6*, 8-15.

[40] H. De-Feng; G. Zhi-Min; G. Wei; M. Jian, Synthesis, Characterization and Electrical Properties of Solid State Electrolyte Materials $La_{2-X}ca_xmo_{1.7}w_{0.3}o_9$-Δ($0 \leqslant X \leqslant 0.2$). *Chin. J. Inorg. Chem.* **2007,** *1* (23), 81-85.

[41] S. A. Hayward; S. A. T. Redfern, Thermodynamic Nature of and Spontaneous Strain Below the Cubic–Monoclinic Phase Transition in $La_2mo_2o_9$. *J Phys: Condens Matter* **2004,** *16* (21), 3571-3583.

[42] G. Corbel; P. Durand; P. Lacorre, Comprehensive Survey of Nd^{3+} Substitution in $La_2mo_2o_9$ Oxide-Ion Conductor. *J Solid State Chem* **2009,** *182* (5), 1009-1016.

[43] X. P. Wang; D. Li; Q. F. Fang; Z. J. Cheng; G. Corbel; P. Lacorre, Phase Transition Process in Oxide-Ion Conductor Beta-$La_2mo_{2-X}w_xo_9$ Assessed by Internal Friction Method. *Appl Phys Lett* **2006,** *89* (2), 021904-021906.

[44] X. P. Wang; Q. F. Fang, Low-Frequency Internal Friction Study of Oxide-Ion Conductor $La_2mo_2o_9$. *J Phys: Condens Matter* **2001,** *13* (8), 1641-1651.

[45] C. Lee, Synthesis and Characterisation of Rare Earth Substituted Bismuth Vanadate Solid Electrolytes. *Solid State Ionics* **1999,** *117* (3-4), 301-310.

[46] J. G. Fletcher, The Ac Impedance Response of the Physical Interface between Yttria-Stabilized Zirconia and $Yba_2cu_3o_{7-X}$. *J Electrochem Soc* **1995,** *142* (8), 2650.

[47] H. Berthou; C. K. Jorgensen, Optical-Fiber Temperature Sensor Based on Upconversion-Excited Fluorescence. *Opt Lett* **1990,** *15* (19), 1100-2.

[48] V. K. Rai, Temperature Sensors and Optical Sensors. *Appl Phys B* **2007,** *88* (2), 297-303.

[49] S. Du; X. Ma; Q. Qiang; G. Zhang; Y. Wang, Emission in $Gd_6o_5f_8$:Yb^{3+},Er^{3+} Micro-Particles for Multimodal Luminescence and Temperature Sensing Upon 980 Nm Excitation. *Phys Chem Chem Phys* **2016,** *18* (38), 26894-26899.

[50] P. Du; L. H. Luo; W. P. Li; Q. Y. Yue; H. B. Chen, Optical Temperature Sensor Based on Upconversion Emission in Er-Doped Ferroelectric $0.5ba(Zr_{0.2}ti_{0.8})O_3$-$0.5(Ba_{0.7}ca_{0.3})Tio_3$ Ceramic. *Appl Phys Lett* **2014,** *104* (15), 152902-152905.

[51] X. Yi; Z. T. Chen; S. Ye; Y. Li; E. H. Song; Q. Y. Zhang, Multifunctionalities of near-Infrared Upconversion Luminescence, Optical Temperature Sensing and Long Persistent Luminescence in $La_3ga_5geo_{14}$:Cr^{3+},Yb^{3+},Er^{3+} and Their Potential Coupling. *Rsc Advances* **2015,** *5* (61), 49680-49687.

[52] X. N. Chai; J. Li; X. S. Wang; Y. X. Li; X. Yao, Color-Tunable Upconversion Photoluminescence and Highly Performed Optical Temperature Sensing in Er^{3+}/Yb^{3+} Co-Doped $Znwo_4$. *Opt Express* **2016,** *24* (20), 22438-22447.

[53] Z. Pan; Y.-Y. Lu; F. Liu, Sunlight-Activated Long-Persistent Luminescence in the near-Infrared from Cr^{3+}-Doped Zinc Gallogermanates. *Nat Mater* **2012,** *11* (1), 58-63.

[54] J. T. S. Irvine; D. C. Sinclair; A. R. West, Electroceramics: Characterization by Impedance Spectroscopy. *Adv Mater* **1990,** *2* (3), 132-138.

Acknowledgements

The author BH gratefully acknowledges the support of the Natural Science Foundation of China (NSFC) for the Youth Scientist grant (Grant No.: NSFC 11504309, NSFC 21771156), and the Early Career Scheme (ECS) fund (Grant No.: PolyU 253026/16P) from the Research Grant Council (RGC) in Hong Kong. The author SY thanks the support of the NSFC (Grant Nos. 21101065) and Guangdong Natural Science Funds for Distinguished Young Scholar (2014A030306009).

Author contributions

B. H. and S. Y. conceived and supervised the research. S. Y. and Q. Z. designed the experiments. Q. H. performed most of the experiments and data analysis. Q. H., X. K., Q. Z. and S. Y. participated in various aspects of the experiments and discussions. M. S. performed the DFT simulations. B.H., M. S., Q. H. and Y. S. wrote the paper. M.S and Q.H contributed equally to this work. All authors discussed the results and commented on the manuscript.

Competing financial interests

The authors declare no competing financial interests.

Graphical Abstract

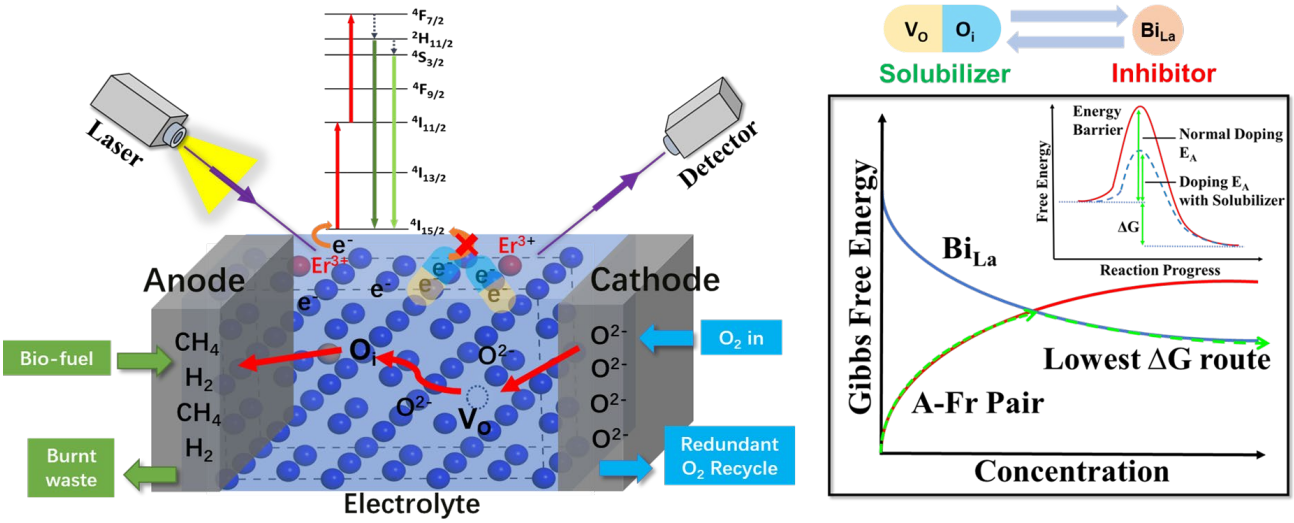

Illustration of non-contact approach to unravel the interaction between intrinsic a-Fr pairs defects and additive Bi dopants in $La_2Mo_2O_9$.

Key word: SOFCs, $La_2Mo_2O_9$, DFT, UC luminescence, Anion-Frenkel pair, Dopant